XLVI CILAMCE
VITÓRIA - ES - BRAZIL - 2025
XLVI IBERO-LATIN AMERICAN CONGRESS ON COMPUTATIONAL METHODS IN ENGENEERING

Exploiting POD-based model order reduction for damped structural dynamics without damped training data

Y. P. Souza[1], F. S. Loureiro[2], D. Soares Jr [3], W. G. Ferreira [4], W. J. Mansur[1]

[1]*LAMEMO/COPPE/Dept. of Civil Engineering, Federal University of Rio de Janeiro*
AV. Pedro Calmon, 21941-596, RJ/Rio de Janeiro, Brazil
yargo.souza@coc.ufrj.br,webe@coc.ufrj.br
[2]*Dept. of Thermal and Fluid Sciences, Federal University of São João del-Rei*
Praça Frei Orlando, 170, 36307-352, MG/São João del-Rei, Brazil
felipe.loureiro@ufsj.edu.br
[3]*Dept. of Structural Engineering, Federal University of Juiz de Fora*
36036-330, MG/Juiz de Fora, Brazil
delfim.soares@ufjf.edu.br
[4]*Dept. of Civil Engineering, Federal University of Espírito Santo*
Avenida Fernando Ferrari, 514, 29075-910, ES/Vitória, Brazil
walnorio@gmail.com

Abstract. The Proper Orthogonal Decomposition (POD) model order reduction technique can identify underlying patterns and reproduce system configurations beyond those present in the training dataset. In this study, we investigate this capability through the simulation of proportional Rayleigh damping matrices, in structural dynamic problems, despite the absence of damping samples in the algorithm's training phase. This aspect of the method remains underexplored, despite its potential to significantly reduce computational effort by avoiding the simulation of the damping matrices in the physical domain (in addition to the computational savings already afforded by the reduced order itself). The proposed strategy is applied to the solution of structural problems discretized via the Finite Element Method (FEM) and time integration methods based on numerical Green's functions (namely, ImGA and ExGA). The results are then compared with those obtained through standard solution approaches.

Keywords: Proper Orthogonal Decomposition, reduced-order model, Rayleigh damping matrix, structural analysis, numerical Green's function

1 Introduction

In the dynamic equilibrium equation, the most difficult term to describe is that related to internal damping forces. For this reason, the most common approach to modeling damping in the Finite Element Method (FEM) is to use the Rayleigh damping matrix [1, 2], rather than the viscous damping matrix, which is seldom employed due to the difficulty in determining an appropriate value for its dissipation constant. In the Rayleigh proportional damping, the damping matrix is approximated by a weighted sum of the mass and stiffness matrices. Due to the additional term in the dynamic equation, simulations that account for physical damping require additional operations, such as matrix-vector multiplications, and consequently involve higher computational costs.

In this work, we model proportional physical damping in structural problems without incurring the additional computational cost typically associated with such simulations using traditional methods. The proposed strategy leverages the learning capability of the Proper Orthogonal Decomposition (POD) technique to generalize beyond the scenarios on which the algorithm was originally trained [3, 4]. The POD is a model order reduction technique [5–8], which has been studied in several areas, including structural dynamics, and is capable of generalizing system behavior beyond the training data. The method consists of projecting the full-order system onto a low-dimensional subspace obtained from a set of representative solutions.

2 Numerical Formulation

2.1 Dynamic equilibrium equation

The semi-discrete equations of motion for elastodynamics originated from the spatial discretization by the Finite Element Method (FEM) are stated as [1]:

$$\mathbf{M}\ddot{\mathbf{U}}(t) + \mathbf{C}\dot{\mathbf{U}}(t) + \mathbf{K}\mathbf{U}(t) = \mathbf{F}(t), \tag{1}$$

$$\mathbf{U}(0) = \mathbf{U}^0, \quad \dot{\mathbf{U}}(0) = \dot{\mathbf{U}}^0, \tag{2}$$

where $\mathbf{M}$, $\mathbf{C}$, $\mathbf{K} \in \mathbb{R}^{m\times m}$ denote, respectively, the mass, damping and stiffness matrices. The vector $\mathbf{U}\,(t) \in \mathbb{R}^m$ contains the m unknown displacement DOFs; moreover, superscript dots denote time derivatives, while $\mathbf{F}\,(t)\in \mathbb{R}^m$ represents the load vector containing the contribution of the prescribed boundary conditions and body forces of the problem under consideration. Finally, vectors $\mathbf{U}^0$, $\dot{\mathbf{U}}^0 \in \mathbb{R}^m$ contain the initial conditions.

Among the terms in eq. (1), the second term, related to internal damping forces, is the most challenging to be defined accurately. Typically, the damping matrix $\mathbf{C}$ is approximated as a linear combination of the mass and stiffness matrices. This approach, known as Rayleigh proportional damping, allows the damping matrix to be constructed assuming that a pair of damping ratios ξ_1 and ξ_2, corresponding to the natural frequencies ω_1 and ω_2, are known. In this case, the Rayleigh damping matrix can be written as:

$$\mathbf{C} = \alpha_1\mathbf{M} + \alpha_2\mathbf{K}, \tag{3}$$

where $\alpha_1 = 2(\omega_1^2\omega_2\xi_2 - \omega_1\omega_2^2\xi_1)/(\omega_1^2 - \omega_2^2)$ and $\alpha_1 = 2(\omega_1\xi_1 - \omega_2\xi_2)/(\omega_1^2 - \omega_2^2)$.

2.2 Model order reduction by POD

To construct the POD basis, dynamic response data is required. This data can be obtained either from measurements or from numerical simulations. If n samples of the solution at the time instants $t_1, \ldots, t_n$ are known, a zero-centered snapshot matrix can be defined as:

$$\bar{\mathbf{U}} = \left[\mathbf{U}(t_1) - \boldsymbol{\mu} \;\cdots\; \mathbf{U}(t_n) - \boldsymbol{\mu}\right], \tag{4}$$

where $\boldsymbol{\mu} = \dfrac{1}{n}\sum_{i=1}^{n}\mathbf{U}(t_i)$.

The Singular Value Decomposition (SVD) of the snapshots matrix leads to [5]:

$$\bar{\mathbf{U}} = \mathbf{L}\boldsymbol{\Lambda}\mathbf{R}^{\mathrm{T}}, \tag{5}$$

where $\mathbf{L} \in \mathbb{R}^{m\times m}$ is the matrix of left singular vectors, whose columns represent the POD modes (spatial basis functions); $\boldsymbol{\Lambda} \in \mathbb{R}^{m\times n}$ is a diagonal matrix containing the singular values $\Lambda_{1,1} \geq \Lambda_{2,2} \geq \cdots \geq \Lambda_{r,r} \geq 0$, with r being the rank of $\bar{\mathbf{U}} \in \mathbb{R}^{m\times n}$; and $\mathbf{R} \in \mathbb{R}^{n\times n}$ is the matrix of right singular vectors, representing the temporal coefficients.

In this work we use the truncated SVD for model order reduction. This approach is particularly suitable because the snapshot matrix $\bar{\mathbf{U}}$ typically has low rank r and the number of degrees of freedom m is much larger than the number of snapshots n (i.e., $m \gg n \geq r$). Under these conditions, the dominant dynamics of the system can be captured accurately using only a few leading POD modes, significantly reducing computational complexity while retaining the essential system behavior.

For the model order reduction, the POD modes can be selected only as the first l columns of $\mathbf{L}$, i.e.:

$$\mathbf{B} = \left[\mathbf{L}_1 \cdots \mathbf{L}_l\right], \tag{6}$$

where $\mathbf{B} \in \mathbb{R}^{m\times l}$ is the new POD basis and l may be selected based on the order p of the energy that the reduced solution will retain [6, 7], according to the following expression:

$$\frac{\sum_{i=1}^{l}\Lambda_{ii}^2}{\sum_{i=1}^{r}\Lambda_{ii}^2} \geq 1 - 10^{-p}. \tag{7}$$

The first l POD modes are expected to be enough to reproduce the behavior of the system. Since the basis components are time-independent, the displacement vector and its time derivatives can be expressed as a linear combination of the reduced basis $\mathbf{B}$ as follows:

$$\mathbf{U}(t) \approx \mathbf{B}\mathbf{U}_l(t), \quad \dot{\mathbf{U}}(t) \approx \mathbf{B}\dot{\mathbf{U}}_l(t), \quad \ddot{\mathbf{U}}(t) \approx \mathbf{B}\ddot{\mathbf{U}}_l(t), \tag{8}$$

with the subscript l in $\mathbf{U}_l(t) \in \mathbb{R}^l$ meaning that the vector is projected onto the reduced space.

Substituting eq. (8) into eq. (1) and eq. (2), premultiplying both sides by $\mathbf{B}^{\mathrm{T}}$ and considering $\mathbf{B}$ orthogonal to the residual generated due to the approximate solutions in a Galerkin projection framework, we obtain the equations of motion for the reduced order model as:

$$\mathbf{M}_l\ddot{\mathbf{U}}_l(t) + \mathbf{C}_l\dot{\mathbf{U}}_l(t) + \mathbf{K}_l\mathbf{U}_l(t) = \mathbf{F}_l(t), \tag{9}$$

$$\mathbf{U}_l(0) = \mathbf{B}^{\mathrm{T}}\mathbf{U}^0, \quad \dot{\mathbf{U}}_l(0) = \mathbf{B}^{\mathrm{T}}\dot{\mathbf{U}}^0, \tag{10}$$

where

$$\mathbf{M}_l = \mathbf{B}^{\mathrm{T}}\mathbf{M}\mathbf{B}, \quad \mathbf{C}_l = \mathbf{B}^{\mathrm{T}}\mathbf{C}\mathbf{B}, \quad \mathbf{K}_l = \mathbf{B}^{\mathrm{T}}\mathbf{K}\mathbf{B}, \quad \mathbf{F}_l(t) = \mathbf{B}^{\mathrm{T}}\mathbf{F}(t), \tag{11}$$

with $\mathbf{M}_l$, $\mathbf{C}_l$, $\mathbf{K}_l \in \mathbb{R}^{l\times l}$ and $\mathbf{F}_l\,(t) \in \mathbb{R}^l$.

The same solution of the FEM can now be reproduced with significantly reduced computational effort. Once the reduced order model solution is obtained with the POD basis, the solution in the physical domain of the finite element mesh can be reconstructed using eq. (8).

2.3 Time domain solution by Green's functions

The discretized solution of eqs. (1)-(2) and eqs. (9)-(10) can be written in terms of the numerical Green's functions yielding distinct time integration methods [3, 4]. In addition, the convolution integral in the velocity expression is manipulated with integration by parts before the numerical approximation. Such procedure has several advantages and allows to establish more efficient explicit and implicit time integration methods, as discussed by Souza et al. [3] and Souza [4]. In this case, the following discretized incremental solution is achieved:

$$\mathbf{U}^{k+1} = \left(\mathbf{G}^1\mathbf{C} + \dot{\mathbf{G}}^1\mathbf{M}\right)\mathbf{U}^k + \mathbf{G}^1\mathbf{M}\dot{\mathbf{U}}^k + \int_0^{\Delta t}\mathbf{G}(\Delta t-\tau)\mathbf{F}(t_k+\tau)d\tau, \tag{12}$$

$$\dot{\mathbf{U}}^{k+1} = \left(\dot{\mathbf{G}}^1\mathbf{C} + \ddot{\mathbf{G}}^1\mathbf{M}\right)\mathbf{U}^k + \dot{\mathbf{G}}^1\mathbf{M}\dot{\mathbf{U}}^k + \mathbf{G}^1\mathbf{F}^k + \int_0^{\Delta t}\mathbf{G}(\Delta t-\tau)\frac{d\mathbf{F}(t_k+\tau)}{d\tau}d\tau, \tag{13}$$

where $\mathbf{U}^k \equiv \mathbf{U}\,(k\Delta t)$, $\mathbf{F}^k \equiv \mathbf{F}\,(k\Delta t)$. In addition, $\mathbf{G}^1 \equiv \mathbf{G}\,(\Delta t)$ and its time derivatives represent the Green's function matrices of the problem under consideration, which here are numerically evaluated.

2.4 Snapshot collection with the ImGA

For the time integration in the snapshot collection, we adopt the ImGA (Implicit Green's functions Approach) [9] where the Green's function in eq. (12) and eq. (13) are computed numerically by the Newmark method and convolutions in the displacement and velocity expressions are approximated by trapezoidal and rectangle rule, respectively, as presented by Souza et al. [3] and Souza [4]. However, in the snapshot collection, we do not consider physical and numerical damping as well. The physical damping with a proportional Rayleigh damping matrix will be included only in the reduced order model to avoiding the numerical effort associated with it. In this case, the following time-marching recurrence expressions for the ImGA arise:

$$\mathbf{U}^{k+1} = 2\mathbf{U}^{k+1/2} - \mathbf{U}^k, \quad \dot{\mathbf{U}}^{k+1} = 2\dot{\mathbf{U}}^{k+1/2} - \dot{\mathbf{U}}^k, \tag{14}$$

where $\dot{\mathbf{U}}^{k+1/2} = c(\mathbf{U}^{k+1/2} - \mathbf{U}^k)$, $c = 2/\Delta t$, and $\mathbf{U}^{k+1/2}$ is obtained by the solution of the effective system:

$$\hat{\mathbf{K}}\mathbf{U}^{k+1/2} = \mathbf{M}(c^2\mathbf{U}^k + c\dot{\mathbf{U}}^k) + \mathbf{F}^{k+1/2}, \tag{15}$$

with the effective stiffness matrix $\hat{\mathbf{K}} = c^2\mathbf{M} + \mathbf{K}$.

2.5 Reduced order model solution with the ExGA

For the reduced order model solution, we use the ExGA (Explicit Green's functions Approach) [10] as presented by Souza et al. [3] and Souza [4]. The method applies the same eqs. (12) and (13); however, Green's functions are now explicitly computed at $t = \Delta t_l$ with s sub-steps of length $h_i = \Delta t_l(j_{i+1} - j_i)$ within the first

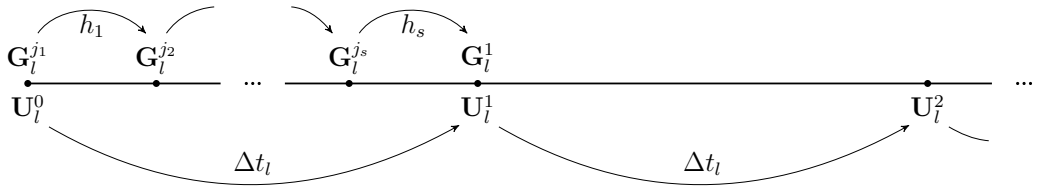


Figure 1. Time integration in the reduced order model for evaluating: (i) the numerical Green's function matrix $\mathbf{G}_l^1$ with s non-equal sub-steps h_i on $s+1$ GLL-points and (ii) displacements $\mathbf{U}_l^k$ with equal time steps Δt_l [3].

time step considering the Gauss-Lobatto-Legenre (GLL) points j_i in the time domain $[0, \Delta t_l]$ (see Fig. 1), and the convolution is approximated with the GLL quadrature rule. In this sense, the ExGA time marching equations ([3, 4]), replacing the term $\dot{\mathbf{G}}_l^1\mathbf{C}_l + \ddot{\mathbf{G}}_l^1\mathbf{M}_l$ by $-\mathbf{G}_l^1\mathbf{K}_l$ [11], can be written as:

$$\mathbf{U}_l^{k+1} = (\mathbf{G}_l^1\mathbf{C}_l + \dot{\mathbf{G}}_l^1\mathbf{M}_l)\mathbf{U}_l^k + \mathbf{G}_l^1\mathbf{M}_l\dot{\mathbf{U}}_l^k + \mathbf{G}_l^*\mathbf{F}_l^*, \tag{16}$$

$$\dot{\mathbf{U}}_l^{k+1} = -\mathbf{G}_l^1\mathbf{K}_l\mathbf{U}_l^k + \dot{\mathbf{G}}_l^1\mathbf{M}_l\dot{\mathbf{U}}_l^k + \mathbf{G}_l^1\mathbf{F}_l^k + \mathbf{G}_l^*\dot{\mathbf{F}}_l^*, \tag{17}$$

where the reduced numerical Green's function matrices $\mathbf{G}_l^{j_{i+1}}$ for each sub-step h_i are evaluated in an explicit manner through the classical fourth-order Runge-Kutta method (Fig. 1) [3, 4] and:

$$\mathbf{F}_l^* = [\mathbf{F}_l^{k+j_{s+1}} \ \cdots \ \mathbf{F}_l^{k+j_1}]^{\mathrm{T}}, \quad \mathbf{G}_l^* = \frac{\Delta t_l}{2}[w_1\mathbf{G}_l^{j_1} \ \cdots \ w_{s+1}\mathbf{G}_l^{j_{s+1}}], \tag{18}$$

where $j_i = (1+\zeta_i)/2$ with $\zeta_i \in [-1, 1]$ denoting the GLL-points obtained by the zeros of $(\zeta^2-1)L_s'(\zeta)$, while w_i are the weights defined as $w_i = 2/\left[s(s+1)L_s^2(\zeta_i)\right]$. Here, L_s is the Legendre polynomial of order s expressed by $L_s(\zeta) = (\mathrm{d}^s(\zeta^2-1)^s/\mathrm{d}\zeta^s)/(2^s s!)$.

For any time step size Δt_l, the method can be arbitrarily more precise once a sufficient large number of sub-steps s is adopted. For instance, in undamped problems the critical time step for one sub-step is $\Delta t_{\mathrm{cr}} = \sqrt{2}/(\pi T_{l,\min})$. However, when multiple sub-steps are used, the method remains stable if the number of sub-steps s is chosen to satisfy at least $s \geq \mathrm{ceil}(\pi\Delta t_l/T_{l,\min})$ [4].

2.6 Algorithm for the proposed strategy

The time integration procedure with order reduction is summarized in Algorithm 1. For snapshot data collection, the ImGA is appropriate due to its low computational cost. In addition, the ImGA is unconditionally stable, second-order accurate, truly self-starting and easy to implement. On the other hand, the ExGA is well-suited for solving the reduced-order model, as it allows the use of a general damping matrix and can achieve high accuracy with just a few POD modes, resulting in minimal computational cost.

Algorithm 1 is designed such that snapshots are collected without damping, while Rayleigh damping is introduced later in the reduced model. In contrast, modeling problems under more than two damping matrices using traditional approaches would require at least two matrix factorizations and additional matrix-vector multiplications involving the damping matrix. These operations significantly increase computational cost, especially for large-scale models (due to the extra factorization) and long time-duration simulations (due to the multiplications). The formulation from Algorithm 1 avoids both of these extra costs, as the snapshots from the undamped model can be reused with different Rayleigh damping matrices in the reduced-order model, with negligible additional computational effort.

3 Numerical Results

3.1 Bar subject to pure tension

A $4\,\mathrm{m}$ long prismatic bar with a $2\,\mathrm{m} \times 2\,\mathrm{m}$ square cross-section is subjected to an impulse load traction at its free end ($z = 4\,\mathrm{m}$), as depicted in Fig. 2. It is assumed that the bar is confined, in such a way that the displacement of the lateral boundaries are restricted in the normal direction [12]. The bar is made of a linear elastic material with Young's modulus $E = 2 \times 10^{11}\,\mathrm{Pa}$, mass density $\rho = 800\,\mathrm{kg/m^3}$, and Poisson's ratio $\nu = 0.25$. It is desired to analyze the displacements at the Point $\mathrm{A}(1\mathrm{m}\,, 1\,\mathrm{m}, 4\,\mathrm{m})$ and Point $\mathrm{B}(1\,\mathrm{m}, 1\,\mathrm{m}, 2\,\mathrm{m})$ for three different damping configurations. The damping ratios ξ_i and ξ_j are known for the natural frequencies $\omega_i = 50\,\mathrm{rad/s}$ and

Algorithm 1 Steps for the POD-Green's functions Approach.

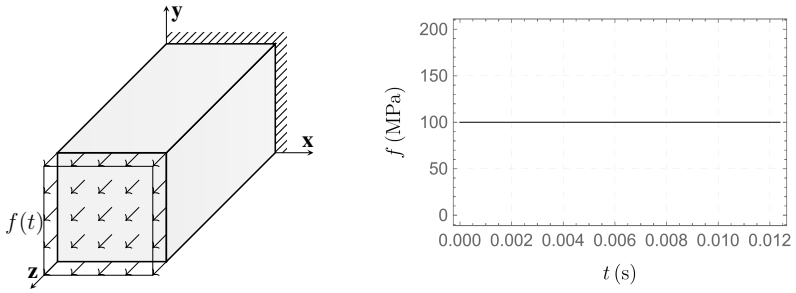
A. *Initial Calculation*.
1. Form stiffness $\mathbf{K}$, mass $\mathbf{M}$, and Rayleigh damping $\mathbf{C}$ matrices and load vector $\mathbf{F}$ (eq. (1)).
2. Set initial conditions $\mathbf{U}^0$ and $\dot{\mathbf{U}}^0$ (eq. (2)).

B. *Snapshots with ImGA without damping*.
1. Select time step Δt and time of analysis t_f.
2. Form the effective stiffness matrix (eq. (15)) and triangularize it as $\hat{\mathbf{K}} = \mathbf{L}\mathbf{D}\mathbf{L}^{\mathrm{T}}$.
3. For each time step Δt: solve for $\mathbf{U}^{k+1/2}$ (eq. (15)) and calculate $\mathbf{U}^{k+1}$ and $\dot{\mathbf{U}}^{k+1}$ (eq. (14)).

C. *Reduced-order model with POD*.
1. Form the snapshot matrix $\bar{\mathbf{U}}$ (eq. (4)).
2. Select the order of retained energy p (eq. (7)).
3. Calculate the left-singular vectors $\mathbf{V}$ and the singular values Λ_{ii} of the snapshot matrix $\bar{\mathbf{U}}$ (eq. (5)).
4. Set the new basis (eq. (6)).
5. Calculate the reduced FEM matrices and load vector (eq. (11)).
6. Set the initial condition vectors for the reduced model (eq. (10)).

D. *Reduced order solution with ExGA^s*.
1. Select the time step Δt_l and number of sub-steps s.
2. Calculate $s+1$ GLL-points ζ_i and weights w_i.
3. For each sub-step $i \in [1, s]$: calculate $\mathbf{G}_l^{j_{i+1}}$ and $\dot{\mathbf{G}}_l^{j_{i+1}}$ on the GLL-points with Runge-Kutta method [3].
4. Calculate $\mathbf{G}_l^*$ (eq. (18)).
5. For each time step Δt_l calculate $\mathbf{F}_l^*$, $\dot{\mathbf{F}}_l^*$, $\mathbf{U}_l^{k+1}$, and $\dot{\mathbf{U}}_l^{k+1}$ (eqs. (16)-(18)).

E. *Project the ROM solution back onto the full-order model* (eq. (8)).

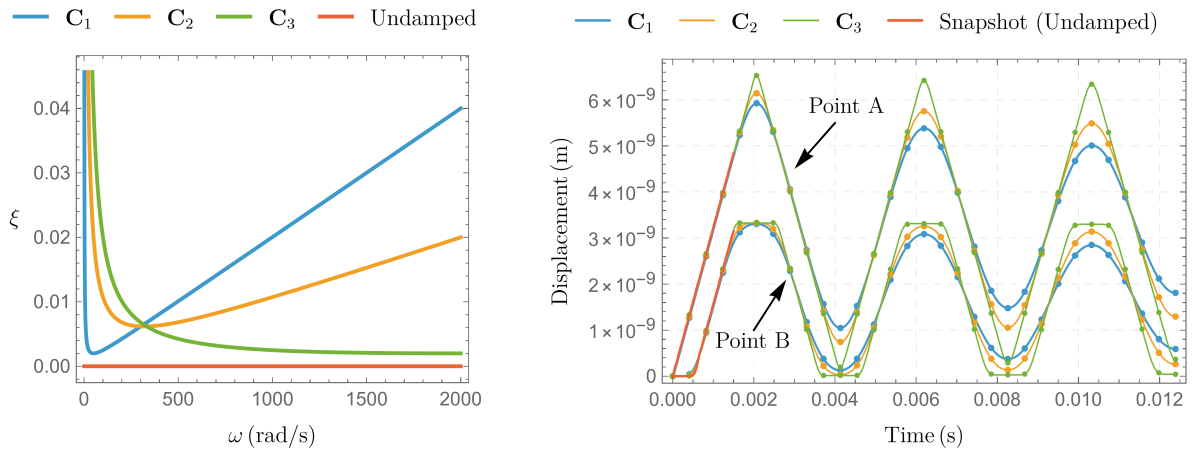


(a) (b)

Figure 2. (a) Bar subject to an axial heaviside loading [3]; (b) Time-dependent function of the loading.

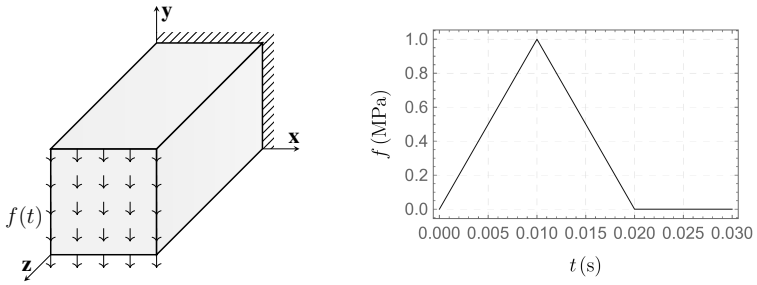
$\omega_j = 2000\,\mathrm{rad/s}$ of the structure. The first damping configuration correspond to the damping ratios $\xi_i = 0.2\%$ and $\xi_j = 4\%$. The second to $\xi_i = 2\%$ and $\xi_j = 2\%$. And the third to $\xi_i = 4\%$ and $\xi_j = 0.2\%$. We model the structural damping with the proportional Rayleigh damping, which results approximately in the following damping matrices according to eq. (3): $\mathbf{C}_1 = 0.1\mathbf{M} + 4\times10^{-5}\mathbf{K}$, $\mathbf{C}_2 = 1.95\mathbf{M} + 1.95\times10^{-5}\mathbf{K}$, and $\mathbf{C}_3 = 4\mathbf{M} + 10^{-6}\mathbf{K}$, for the first, second, and third damping configurations, respectively. The distribution of the damping ratios across different natural frequencies for each Rayleigh damping configuration is presented in Fig. 3 (a). The bar is discretized into 1024 hexahedron elements with 20 nodes each. The reference solution obtained by the Newmark method with the time step $\Delta t = 3\times10^{-6}$ s for a time of analysis of $t_f = 1.2393\times10^{-2}$ s is plotted in Fig. 3 (b).

For the POD approach, the snapshots are collected with no physical damping by the ImGA. A time step of $\Delta\bar{t} = 3\times10^{-5}$ s for a total simulation time of $\bar{t}_f = 3\times10^{-3}$ s proved to be sufficient to capture the system behavior. Then, the reduced-order model was built with only $l = 25$ POD modes ($p = 6$) obtained from the SVD of the snapshots. Finally, the reduced-order model was solved by the ExGA with a large time step $\Delta t_l = 4.1312\times10^{-4}$ s for the first, second and third damping conditions, only in the reduced-order model, i.e., it was imposed the damping matrices $\mathbf{C}_1$, $\mathbf{C}_2$, and $\mathbf{C}_3$ projected onto the 25 POD modes, as the $\mathbf{C}_l$ matrix defined in eq. (11). In order to ensure a highly accurate solution (including the convolution approximations), in this example as well as in the next one, the number of sub-steps is set to $s = 100$. In the reduced-order model it is possible to increase the number sub-steps without significantly increase the computational effort. The results are plotted in Fig. 3 (b) and are in excellent agreement with the reference solution.



(a) (b)

Figure 3. (a) Frequency variation of the damping ratios for the Rayleigh matrices $\mathbf{C}_1$, $\mathbf{C}_2$, and $\mathbf{C}_3$; (b) Time-dependent displacements with the Newmark method (solid line) and POD-Green's function Approach (dots).



(a) (b)

Figure 4. (a) Bar subject to a dynamic shear loading; (b) Time-dependent function of the loading.

3.2 Bar subject to a shear loading

Now assume a clamped-free bar with the same dimensions and damping conditions of the previous example is subjected to a shear dynamic loading at its free end ($z = 4\,\text{m}$), as illustrated in Fig. 4. The material properties are given by $E = 10^5$ Pa, $\rho = 1$ kg/m^3, and $\nu = 0.25$ [12]. The reference solution is obtained once again by the Newmark method with $\Delta t = 1.5 \times 10^{-4}$ s and $t_f = 0.3$ s. The snapshots are collected without physical damping by the ImGA with $\Delta\bar{t} = 1.5 \times 10^{-3}$ s and $\bar{t}_f = 0.05$ s. Then, the reduced-order model is built with $l = 10$ POD modes ($p = 6$) obtained from the SVD of the snapshots. Finally, the reduced-order model is solved by the ExGA with the time step $\Delta t_l = 0.025$ s with the results being presented in Fig. 5.

It is important to remark that for the two numerical experiments, an efficient snapshot collection, with maximal time step length $\Delta\bar{t}$ and minimal time of analysis $\bar{t}_f$, is achieved when the rank of the snapshot matrix r approaches the number of samples n. Moreover, the snapshot collection without the damping matrix can be used to reproduce the solution under different Rayleigh damping matrices. Even if it were necessary for the snapshot to cover the entire time span of analysis, the use of a larger time step and/or the ability to collect snapshots under different damping conditions ensures that the POD approach is more efficient than standard methods in terms of the use of computational resources. For a quantitative comparison of the increase in accuracy and computational speedup with POD-Green's functions Aproach see Souza et al. [3] and Souza [4].

4 Conclusions

This paper designed a strategy to avoid the additional computational effort associated with imposition of the proportional damping matrices. The strategy used the POD with models trained without physical damping to simulate an arbitrary Rayleigh damping matrix. The physical damping is incorporated only in the reduced-order model with negligible computational cost. In the numerical examples the POD-Green's functions Approach successfully obtained the structural response with low computational effort and high accuracy for different Rayleigh damping

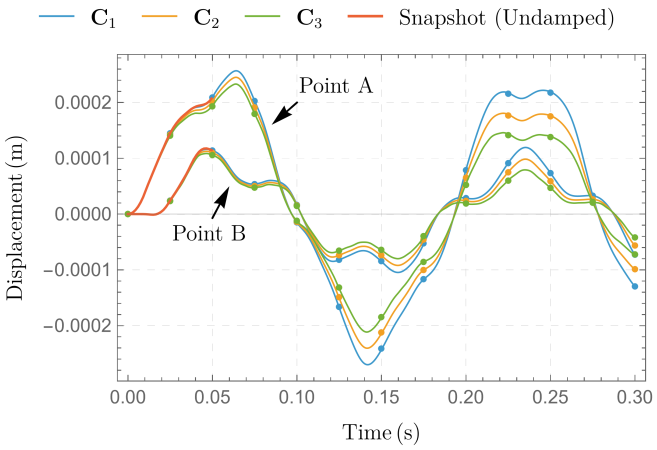


Figure 5. Time-dependent displacements with the Newmark method (solid line) and POD-Green's function Approach method (dots) for the Rayleigh matrices $\mathbf{C}_1$, $\mathbf{C}_2$, and $\mathbf{C}_3$.

matrices without assume physical damping in the full-order model.

Acknowledgements. The authors acknowledge support of Coordenação de Aperfeiçoamento de Pessoal de Nível Superior - Brasil (CAPES), UFSJ/PPMEC/DCTEF, CNPq, FAPERJ, PETROBRAS (CENPES), and FAPEMIG.

Authorship statement. The authors hereby confirm that they are the sole liable persons responsible for the authorship of this work, and that all material that has been herein included as part of the present paper is either the property (and authorship) of the authors, or has the permission of the owners to be included here.

References

[1] K. Bathe. *Finite element procedures*. Prentice-Hall, New Jersey, second edition edition, 2014.
[2] A. K. Chopra. *Dynamics of structures: Theory and applications to earthquake engineering*. Prentice-Hall, Englewood Cliffs, 1995.
[3] Y. Souza, F. Loureiro, W. Mansur, W. Ferreira, and R. Camargo. A time-domain pod approach based on numerical implicit and explicit green's functions for 3d elastodynamic analysis. *Computers & Structures*, vol. 275, pp. 106921, 2023.
[4] Y. Souza. *Uma abordagem POD no domínio do tempo baseada em funções de Green Numéricas para elastodinâmica 3D via MEF*. PhD thesis, Universidade Federal do Rio de Janeiro, 2023.
[5] S. L. Brunton and J. N. Kutz. *Data-driven science and engineering: Machine learning, dynamical systems, and control*. Cambridge University Press, 2022.
[6] S. E. Azam and S. Mariani. Investigation of computational and accuracy issues in POD-based reduced order modeling of dynamic structural systems. *Engineering structures*, vol. 54, pp. 150–167, 2013.
[7] L. Sirovich. Turbulence and the dynamics of coherent structures. Part I: Coherent structures. *Quarterly of applied mathematics*, vol. 45, n. 3, pp. 561–571, 1987.
[8] K. Pearson. On lines and planes of closest fit to systems of points in space. *The London, Edinburgh, and Dublin Philosophical Magazine and Journal of Science*, vol. 2, n. 11, pp. 559–572, 1901.
[9] D. Soares and W. Mansur. A time domain fem approach based on implicit green's functions for non-linear dynamic analysis. *International Journal for Numerical Methods in Engineering*, vol. 62, n. 5, pp. 664–681, 2005.
[10] W. J. Mansur, F. Loureiro, D. Soares Jr, and C. Dors. Explicit time-domain approaches based on numerical green's functions computed by finite differences–the exga family. *Journal of Computational Physics*, vol. 227, n. 1, pp. 851–870, 2007.
[11] F. Loureiro and W. Mansur. An efficient hybrid time-laplace domain method for elastodynamic analysis based on the explicit green's approach. *International Journal of Solids and Structures*, vol. 46, n. 16, 2009.
[12] M. H. Aliabadi. *The boundary element method, volume 2: applications in solids and structures*, volume 2. John Wiley & Sons, 2002.